

REFRACTIVE INDICES DETERMINATION OF A NEW NEMATIC LIQUID CRYSTAL

I. Palarie*, C. Florea^a

Faculty of Physics, University of Craiova, 13 A. I. Cuza Str., Craiova-200585, Romania

^aLaboratoire de Signaux et de Télécommunications (SIGTEL) de l'ESIEE – Paris
BP 99, 2 bd. Blaise Pascal, 93162 NOISY-LE-GRAND cedex France

We report the determination of the refractive indices of a new nematic liquid crystal 4'-cyano-(4-chlor-benzyloxy)-azobenzene, within the spectral range [570 – 800] nm for various temperatures pertaining to the nematic phase range of [159.1 – 183] °C. In order to obtain the ordinary and extraordinary refractive indices, the wavelength dependence of the light intensity transmitted by the cell, filled with this nematic liquid crystal, has been recorded at various temperatures with respect to the incidental beam light, polarized orthogonal to, respectively parallel with the optical axis. By using the three-band model and a nonlinear fitting procedure, from the wavelength dependence of the transmitted light intensity we have obtained the parameters involved in the expressions of the refractive indices and we have computed the refractive indices.

(Received February 21, 2005; accepted March 23, 2005)

Keywords: Liquid crystals, Refractive indices, Optical birefringence

1. Introduction

Nematic liquid crystals (NLCs) locally behave like uniaxial anisotropic media. The optical birefringence, defined like $\Delta n = n_e - n_o$, is large, around 0.2 and can be easily controlled through the variation of the temperature and/or external field. In the above, n_e represents the principal extraordinary refractive index, hence corresponding to a light beam polarization parallel to the optical axis, while n_o denotes the ordinary refractive index, associated with a light beam polarization orthogonal to the optical axis.

Many studies have been devoted to refractive indices measurements of liquid crystals using an Abbe refractometer [1-3], the hollow prism technique [4,5] and the wedge method [6], a Jellay-Leitz refractometer [7], the interference method for plane-parallel nematic cell [8], the shearing method [9] and also the Talbot-Rayleigh method [10-12].

Much work has been done to investigate the physical origin of the refractive index dispersions of liquid crystals [13-16]. The three-band model [15] is a realistic model, in a good agreement with the experimental data obtained by S. T. Wu and his collaborators [15,16]. The accuracy of this model for (p-etoxybenzylidene)-p-n-butylaniline (EBBA) has been confirmed in a recent paper by M. Socaciu and M. Ursache [12]. In the framework of this model, one considers a single $\sigma \rightarrow \sigma^*$ transition (designated as the λ_0 -band, located in the vacuum UV region, $\lambda_0 \sim 120$ nm) and two $\pi \rightarrow \pi^*$ transitions (designated as the λ_1 - and λ_2 -bands, with $\lambda_2 > \lambda_1$ placed in the nearby-ultraviolet and obtained by using the absorption spectrum of the liquid crystal under study).

For this model, in the visible and infrared regions where $\lambda \gg \lambda_0$, n_e and n_o are expressed as:

* Corresponding author: palarie@central.ucv.ro

$$n_{e,o}(\lambda, t) = 1 + n_{0e,o}(t) + g_{1e,o}(t) \frac{\lambda^2 \lambda_1^2}{\lambda^2 - \lambda_1^2} + g_{2e,o}(t) \frac{\lambda^2 \lambda_2^2}{\lambda^2 - \lambda_2^2}, \quad (1)$$

where λ is the wavelength of light, t denotes the temperature of the NLC and $n_{0e,o}$, $g_{1e,o}$ and $g_{2e,o}$ represent six parameters which are temperature-dependent [15].

The cell employed by us has been constructed from two semitransmitting glass plates (SGPs). A solution of poly(vinyl alcohol) and water (3:100) was spin coated on the SGPs at room temperature and at a turning speed of 2000 rot/min [17]. The thin polymeric film, with a thickness of about 100 nm [17] has been baked in an oven at 120 °C for an hour. Subsequently, the thin film has been rubbed along a given direction in order to ensure a planar alignment of the NLC along the rubbing direction. The two semitransmitting glass plates composing the cell have been separated by Mylar spacers and then attached by Unimetal epoxidic resine, resisting up to 250 °C. In order to determine the thickness “d” of the cell (the distance between the inner faces of the cell plates) we have recorded the wavelength dependence of the light intensity transmitted by the empty cell. The thickness of the cell (16720 ± 1 nm) has been computed according to a one-parameter Levenberg-Marquardt nonlinear fitting (LMNF) procedure (the parameter is nothing but the cell thickness), by taking into account the reflectance $R(\lambda)$ and the transmittance $T(\lambda)$ of the SGPs covered with the polymeric film.

The measurements for the cell filled with 4'-cyano-(4-chlor-benzyloxy)-azobenzene (denoted by 4CN) have been realized by using an original experimental setup. The physical model chosen to describe the wavelength dependence of the refractive indices is the three-band model. The choice of this model is motivated by the fact that we already had by hand the UV absorption spectrum of 4CN. In order to determine the refractive indices $n_o(\lambda, t)$ and $n_e(\lambda, t)$ we have placed the cell filled with the nematic sample planary aligned between two polarizers with parallel transmission directions. The optical axis of the 4CN NLC has been positioned orthogonal to, respectively parallel with the transmission direction of the polarizers. For each of these fixed positions of the optical axis we have recorded the wavelength dependence of the light intensity transmitted by the cell at various temperatures “t” (160, 165, 170, 175, 180) °C within the nematic phase range. Four parameters have been used during the nonlinear fitting procedure of the wavelength dependence of the transmitted light intensity. Three of them are those appearing in the expressions of the refractive indices from the three-band model, while the fourth is the thickness of the cell. In this way we reach an excellent agreement between the values of the thickness of the cell in the empty and respectively filled with 4CN cases, resulting from the two nonlinear fitting procedures (one- and respectively four-parameters techniques). The first three fitting parameters were employed at the computation of the ordinary ($n_o(\lambda, t)$) and extraordinary ($n_e(\lambda, t)$) refractive indices at these temperatures in a spectral range of [570-800] nm. The comparison of the values of the optical birefringence $\Delta n(\lambda, t)$ obtained by means of subtracting $n_o(\lambda, t)$ from $n_e(\lambda, t)$ with those resulting by direct measurements [18] provided a good agreement.

2. Experimental method and results

2.1 Experimental method of measuring the thickness of a sandwich-type cell taking into account the transmittance and the reflectance of the parallel semitransmitting glass plates

Initially, we determine the thickness “d” of the empty cell. As the cell is meant to behave as a Fabry-Pérot resonator it is necessary to determine, also, the wavelength-dependence of both transmittance $T(\lambda)$ and reflectance $R(\lambda)$ of the SGPs composing the cell. The reflectance $R(\lambda)$ of the SGP at normal incidence angle, is determined by recording, with an Ocean Optics Spectrometer S 2000, of both spectral distribution of the LS-1 Tungsten Halogen light source at normal incidence on the SGP, and the spectral distribution of the reflected light. The transmittance $T(\lambda)$ of the SGP is determined through the spectral distribution of the light source at normal incidence on the SGP combined with the spectral distribution of the transmitted light. The wavelength-dependence of both $T(\lambda)$ and $R(\lambda)$ for the SGPs is presented in Fig. 1.

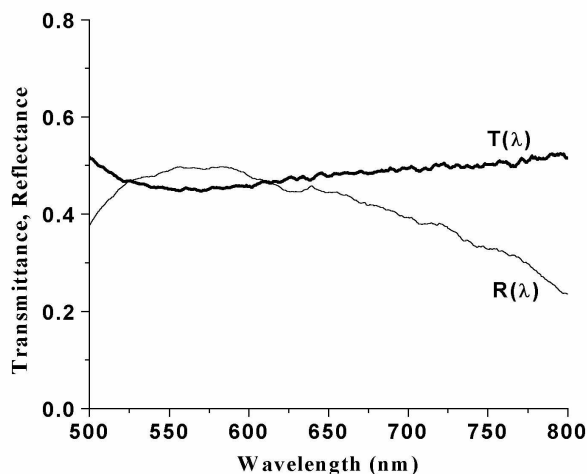


Fig. 1. Wavelength-dependence of transmittance and reflectance for the SGPs.

In order to determine the thickness “d” of the empty cell, the experimental setup presented in Fig. 2 has been used.

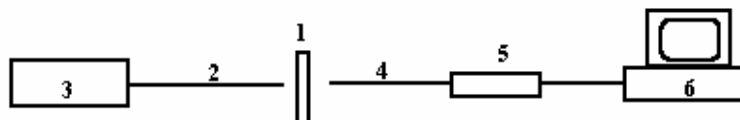


Fig. 2. Experimental setup for empty cell thickness measurements.

The cell (1) is empty. The LS-1 Tungsten Halogen light source (3) has a spectral range of 360-2000 nm. The parallel beam emerging from the optical fiber (2) is at normal incidence on the cell. The transmitted light comes to Ocean Optics Spectrometer S 2000 (5) through the optical fiber (4). The computer (6) has a National Instruments interface. The wavelength-dependent transmitted intensity of the empty cell is presented in Fig. 3 (only within the 500-800 nm range).

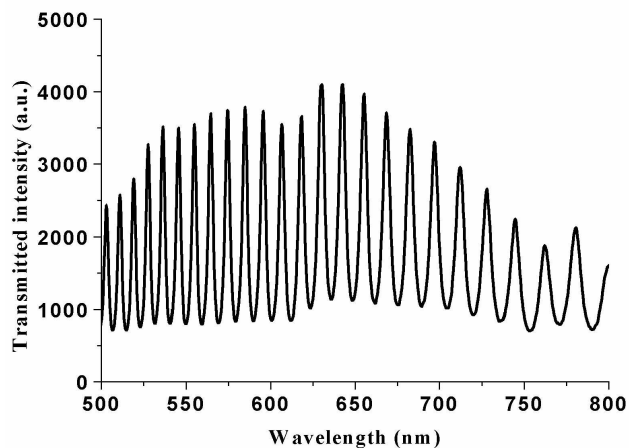


Fig. 3. Wavelength-dependent transmitted intensity of the empty cell.

In the ideal case, the transmitted intensity $I_T(\lambda)$ is given by:

$$I_T(\lambda) = I_I(\lambda) \left(\frac{T(\lambda)}{1-R(\lambda)} \right)^2 \frac{1}{1 + \frac{4R(\lambda)}{(1-R(\lambda))^2} \sin^2\left(\frac{2\pi d}{\lambda}\right)}, \quad (2)$$

where $I_I(\lambda)$ is the incident beam intensity on the cell at a wavelength λ , d means the thickness of the empty cell, $R(\lambda)$ represents the reflectance, while $T(\lambda)$ signifies the transmittance of the SGP. The channeled aspect of the transmitted intensity is exclusively due to the presence of the factor $\sin^2(2\pi d / \lambda)$. The intensity of the incidental light beam $I_I(\lambda)$ has been recorded in the absence of the cell.

During our experiment, we must pay attention to several factors, like the dark signal $D(\lambda)$, the spectral distribution of the lamp, and also the spectral sensitiveness of the spectrometer. The most important of them is the dark signal $D(\lambda)$, which is obtained by switching off the light source. Therefore, we should, accordingly, modify the relation (2) as follows:

$$\sin^2\left(\frac{2\pi d}{\lambda}\right) \propto \frac{\frac{I_I(\lambda) - D(\lambda)}{I_T(\lambda) - D(\lambda)} \left(\frac{T(\lambda)}{1-R(\lambda)} \right)^2 - 1}{\frac{4R(\lambda)}{(1-R(\lambda))^2}} \equiv E(\lambda) \quad (3)$$

Using a LMNF procedure, we then determine the thickness “ d ” of the cell, which actually is the only one-fitting parameter. In Fig. 4 the solid line indicates the right-hand side of the relation (3), while the dashed line signifies the result of the fitting procedure. Since the input to the nonlinear fitting procedure consists in a large number of points (≈ 270) in a narrow wavelength range (90 nm), the thickness d of the cell will be determined with a high accuracy: $d = 16720 \pm 1$ nm. Once a certain measurement of the thickness has been completed, the corresponding area is marked on one of the SGPs for a proper correlation with the measurements of the n_e and n_o .

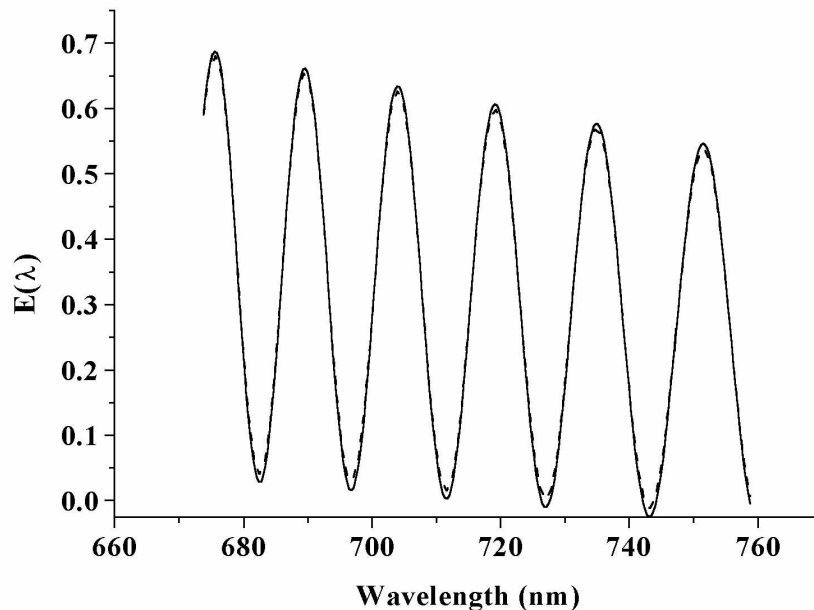


Fig. 4. Determination of the thickness d of the empty cell using the LMNF procedure ($d = 16720 \pm 1$ nm).

2.2 Structural formula, absorption spectrum and nematic phase range of 4CN

4CN is also known as 4-chlor-phenilen-metilen-4-oxy-4'-cyano-azobenzene [19] and 4-[(4-chlorobenzyl)oxy]-4'-cyanoazobenzene [20]. It has been recently synthesized [20] and studied [18,19]. The polymorphism of the 4CN was studied by microstructural analysis in polarized light and differential thermal analysis [19]. This substance exhibit the nematic phase while heating within the $[159.1 \rightarrow 183]^{\circ}\text{C}$ range and while cooling within the $[143 \leftarrow 181]^{\circ}\text{C}$ range [19]. Its structural formula is given in Fig. 5. The UV absorption spectrum (Fig. 6) of a solution 0.01% of 4CN dissolved in ethylic alcohol was obtained via an Ocean Optics Spectrometer S 2000. We remark the absorption bands $\lambda_1 = 248.17$ nm and $\lambda_2 = 358.90$ nm.

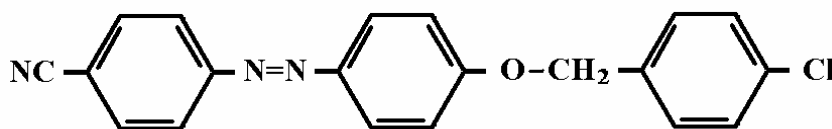


Fig. 5. Structural formula of 4CN.

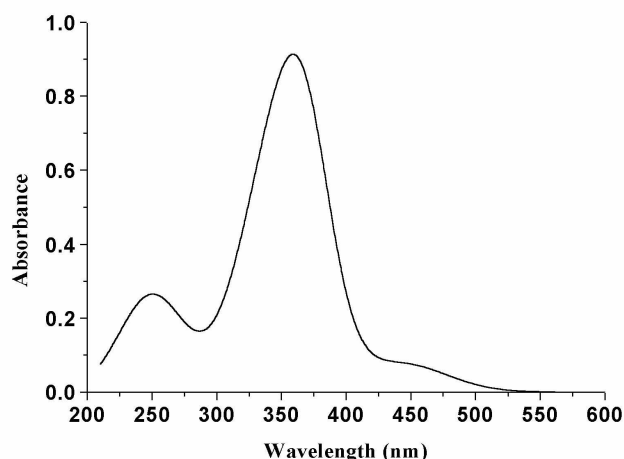


Fig. 6. Absorption spectrum of 4CN.

2.3 The orientation of the local optical axis and the principal refractive indices of 4CN

The sandwich-type cell was filled by capillarity with 4CN. The experimental setup is presented in Fig. 7.

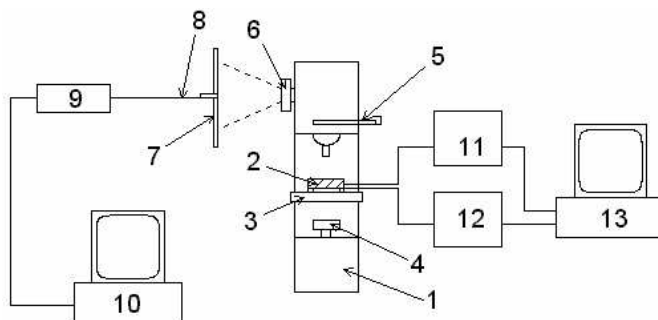


Fig. 7. Experimental setup for the measurement of the principal refractive indices of NLC.

The cell is placed within a special electric oven (2), which is connected to a temperature controller (12), allowing the sample to be cooled and heated at a $1^\circ\text{C}/\text{min}$ linear temperature rate. The temperature was measured with a Constantan-Copper thermocouple connected to a KEITHLEY 2000 multimeter of 0.01°C precision (11). The computer (13) has two interfaces: DAS 1601 and IEEE 488. The oven is placed on the table (3) of an IOR-MC5A microscope (1). The sample was illuminated with white light from a quartz-Halogen lamp. The experimental setup also contains a polarizer (4) and an analyzer (5). The output image is displayed on the screen (7) by using the device (6). The optical fiber (8) has a small diameter, of $400\ \mu\text{m}$, which allows for a local measurement on the sample, of about $4\ \mu\text{m}$ in diameter. The spectrometer (9) is connected to the computer (10) via a National Instruments interface. The cell has been heated up to a certain temperature within the nematic range.

2.3.1 The orientation of the local optical axis

The polarizer and the analyzer are oriented parallel one to the other. In order to determine the orientation of the local optical axis with respect to the polarizers, we rotate the cell and search the two positions of the cell for which the differences between the maxima and minima becomes highest, which are obviously orthogonal. These two positions correspond to the optical axis oriented parallel and orthogonal to the transmitted axis of the polarizers. As we work with a positive anisotropic uniaxial NLC ($n_e > n_o$) [18], it follows that the position corresponding to a higher density of channels will be associated with a local optical axis parallel to the polarizers, while that with a lower density will automatically induce an optical axis orthogonal to them.

2.3.2 Ordinary refractive index of 4CN

The sample, with planar orientation, is maintained with its optical axis perpendicular to the transmitted axis of the polarizers in order to determine n_o . The transmitted light is analyzed using the spectrometer at various temperatures ($160, 165, 170, 175, 180^\circ\text{C}$), within the nematic phase range, by heating the sample with $1^\circ\text{C}/\text{min}$. In the absence of the cell we record the intensity $I_T(\lambda)$. The dark signal $D(\lambda)$ is obtained by switching off the quartz-Halogen lamp. We expose in Figs. 8 and 9 the wavelength-dependent ordinary transmitted intensity of 4CN at 160°C and 180°C , respectively. We obtain 33 transmission maxima at 160°C and 34 transmission maxima at 180°C in the $550\text{-}800\ \text{nm}$ range. The increasing of the number of maxima reveals that n_o slightly increases as the temperature increases. As the maxima density decreases when the wavelength increases, we conclude that we are dealing with a normal dispersion.

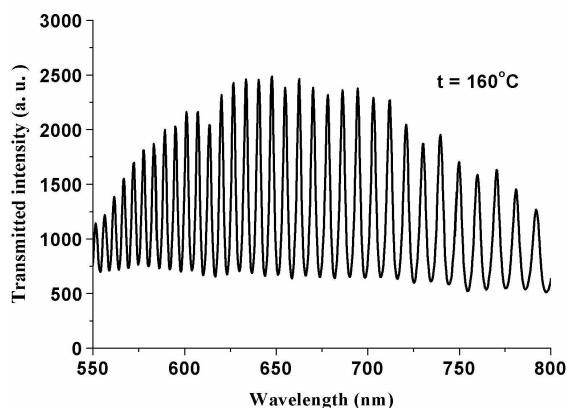


Fig. 8. Wavelength-dependent ordinary transmitted intensity at 160°C .

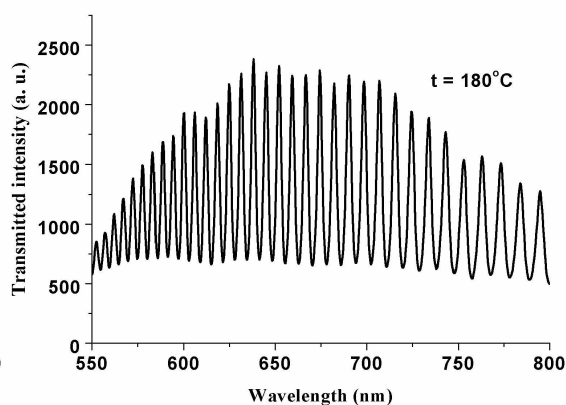


Fig. 9. Wavelength-dependent ordinary transmitted intensity at 180°C .

The ordinary transmitted intensity $I_{T_o}(\lambda, t)$ in the ideal case is expressed by:

$$I_{T_o}(\lambda, t) = I_I(\lambda) \left(\frac{T'(\lambda)}{1-R'(\lambda)} \right)^2 \frac{1}{1 + \frac{4R'(\lambda)}{(1-R'(\lambda))^2} \sin^2 \left(\frac{2\pi d \cdot n_o(\lambda, t)}{\lambda} \right)} \quad (4)$$

where $R'(\lambda)$ and $T'(\lambda)$ are the reflectance and respectively the transmittance in the case of the cell filled with 4CN, for the SGPs covered with polymeric film.

By taking into account that $n_o \sim 1.5$ and that the refractive index of poly(vinyl alcohol) has an order of magnitude of 1.52 [21], after some computation we find that the difference between $R'(\lambda)$ and $R(\lambda)$ is less than 6% of $R(\lambda)$, a difference of the same order of magnitude being observed also between $T'(\lambda)$ and $T(\lambda)$.

Based on the above estimations, we get

$$\left(\left(\frac{T(\lambda)}{1-R(\lambda)} \right)^2 - \left(\frac{T'(\lambda)}{1-R'(\lambda)} \right)^2 \right) / \left(\frac{T(\lambda)}{1-R(\lambda)} \right)^2 < 1\%, \quad (5)$$

so we are allowed make the approximations $\left(\frac{T'(\lambda)}{1-R'(\lambda)} \right)^2 \cong \left(\frac{T(\lambda)}{1-R(\lambda)} \right)^2$.

On the other hand, from the same observations it results

$$\left(\frac{R(\lambda)}{(1-R(\lambda))^2} - \frac{R'(\lambda)}{(1-R'(\lambda))^2} \right) / \left(\frac{R(\lambda)}{(1-R(\lambda))^2} \right) \cong 14\%, \quad (6)$$

which, also significant in value, is however not essential for the fitting procedure, since it can be compensated by a proper rescaling operation.

Consequently, we can finally modify the relation (4) as follows:

$$\sin^2 \left(\frac{2\pi d \cdot n_o(\lambda, t)}{\lambda} \right) \propto \frac{I_I(\lambda) - D(\lambda) \left(\frac{T(\lambda)}{1-R(\lambda)} \right)^2 - 1}{\frac{4R(\lambda)}{(1-R(\lambda))^2}} \equiv F(\lambda) \quad (7)$$

Using a LMNF procedure and the three-band model, we determine the parameters $n_{o_0}(t)$, $g_{1_0}(t)$ and $g_{2_0}(t)$ involved with the computation of $n_o(\lambda, t)$ and the thickness “d” of the cell, which is a new parameter P. We are thus able to determine the dispersion of n_o for 4CN at these temperatures.

In Fig. 10 we give the fitting procedure result at a temperature of 170 °C. The solid line indicates the experimental result, while the dashed line shows the result of the fitting procedure. The fitting procedure has led to a value of 16721 ± 8 nm, corresponding to the parameter P, playing the role of the cell thickness, which is very close to the value (16720 ± 1 nm) determined in the above in the case of the empty cell. This grants on the one hand that we performed the measurements of n_o and n_e at the correct area marked on the SGP, and on the other hand that the output value of the three parameters are reliable.

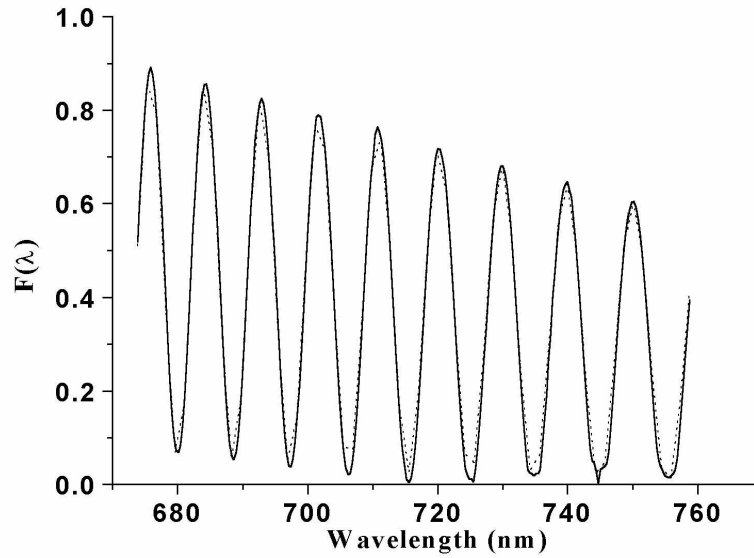


Fig. 10. Determination of the parameters n_{0o} , g_{1o} , g_{2o} and P using the LMNF procedure.

The fitted parameters $n_{0o}(t)$, $g_{1o}(t)$ and $g_{2o}(t)$ obtained for various temperatures are given in Table 1. Using the data listed in Table 1 and the relation (1), we obtain the wavelength-dependent n_o at these temperatures, see Fig. 11. The n_o decreases as the wavelength increases at a fixed temperature, and also increases as the temperature increases at a fixed wavelength.

Table 1. Ordinary refractive index of 4CN: Fitted parameters n_{0o} , g_{1o} , g_{2o} , and χ^2 (chi-square) at various temperatures.

Temperature ($^{\circ}\text{C}$)	n_{0o}	g_{1o} (10^{-6} nm^{-2})	g_{2o} (10^{-7} nm^{-2})	χ^2 (10^{-4})
160	0.39690	1.1890	3.9170	3.15
165	0.39812	1.1887	4.0902	3.20
170	0.40776	1.1926	4.1020	2.60
175	0.41250	1.2235	4.1071	4.10
180	0.42131	1.2418	4.2163	3.06

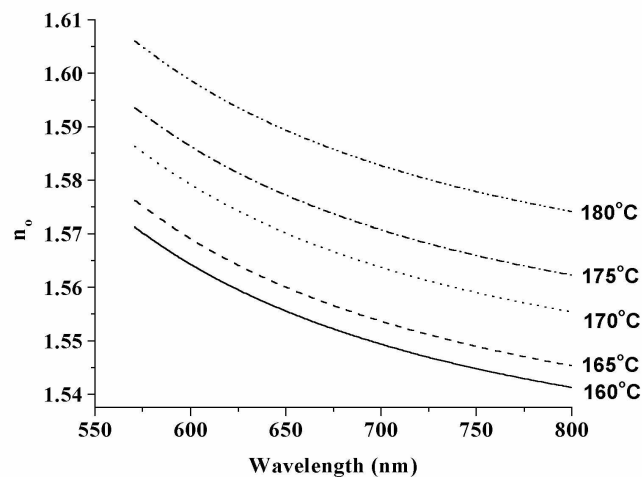


Fig. 11. n_o versus λ at various temperatures.

2.3.3 Extraordinary refractive index of 4CN

In this case, the optical axis is parallel to the transmitted axis of the polarizers. The sample has been heated by 1°C/min. We record the wavelength-dependent extraordinary transmitted intensity of 4CN at different temperatures (160, 165, 170, 175, 180) °C. We obtain 39 transmission maxima at 160 °C (Fig. 12) and 38 transmission maxima at 180 °C (Fig. 13) within the 570-800 nm range. The decreasing of the number of maxima reveals that n_e decreases as the temperature increases.

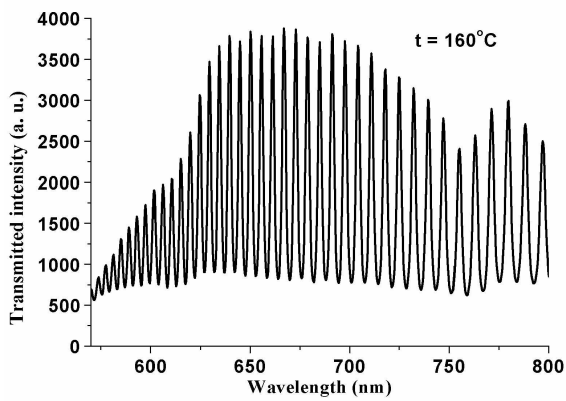


Fig. 12. Wavelength-dependent extraordinary transmitted intensity at 160 °C.

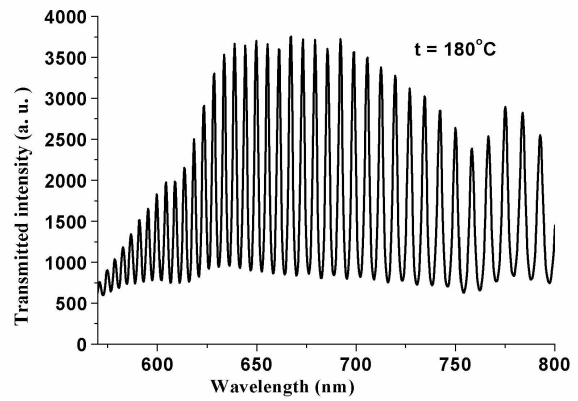


Fig. 13. Wavelength-dependent extraordinary transmitted intensity at 180 °C.

Using the same procedure as in the case of n_o , we determine the parameters $n_{0e}(t)$, $g_{1e}(t)$ and $g_{2e}(t)$, see Table 2.

Table 2. Extraordinary refractive index of 4CN: Fitted parameters n_{0e} , g_{1e} , g_{2e} , and χ^2 at various temperatures.

Temperature (°C)	n_{0e}	g_{1e} (10^{-6} nm^{-2})	g_{2e} (10^{-6} nm^{-2})	χ^2 (10^{-5})
160	0.46878	2.1090	1.0553	4.15
165	0.46791	2.1087	1.0497	3.82
170	0.46498	2.1096	1.0483	2.00
175	0.45479	2.0845	1.0400	5.80
180	0.44030	1.7730	1.0325	2.06

The wavelength-dependent n_e at these temperatures is presented in Fig. 14. The n_e decreases as the wavelength increases at a fixed temperature, and also decreases as the temperature increases at a fixed wavelength.

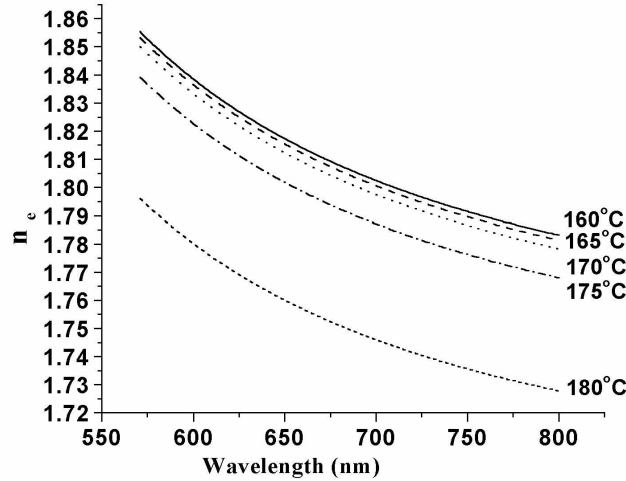


Fig. 14. n_e versus λ at various temperatures.

3. Discussion

Using the wavelength-dependent n_e and n_o of the 4CN at various temperatures, we can determine the corresponding wavelength-dependent birefringence through:

$$\Delta n(\lambda, t) = n_e(\lambda, t) - n_o(\lambda, t) \quad (8)$$

Alternatively, we can gain $\Delta n(\lambda, t)$ directly, by maintaining the optical axis of the NLC at $\pi/4$ to the crossed polarizers. In Fig. 15 we expose the results obtained by using both methods at a fixed temperature of 170 °C. The solid line is the optical birefringence obtained directly [18], and the dashed line shows the result based on the relation (8). At $\lambda = 633$ nm, we get $\Delta n = 0.2467$ from the direct method, and $\Delta n = 0.2450$ via n_e and n_o , which allows us to conclude that there is a good agreement between these methods.

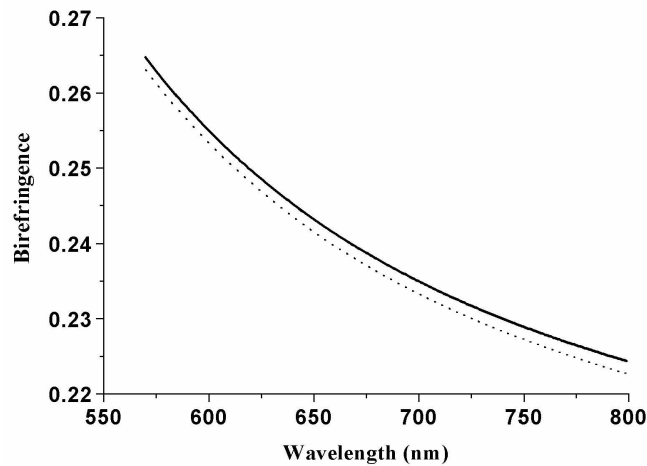


Fig. 15. Birefringence versus wavelength at 170 °C using these two methods.

4. Conclusions

The refractive indices of a new nematic liquid crystal 4'-cyano-(4-chlor-benzyloxy)-azobenzene have been determined by using an interference method for the plane-parallel nematic cell. The cell employed here has been constructed from two SGPs covered with a thin film of poly(vinyl alcohol). The reflectance and transmittance of the SGPs have been determined and used in order to obtain the refractive indices $n_o(\lambda, t)$ and $n_e(\lambda, t)$ from the wavelength dependence of the light intensity transmitted by the cell filled with 4CN at various temperatures with respect to the incidental beam light, polarized orthogonal to, respectively parallel with the optical axis. By using the three-band model and a nonlinear fitting procedure, from these dependences we have obtained the parameters involves in the expressions of the refractive indices. The comparison between the values of the optical birefringence $\Delta n(\lambda, t)$ obtained by means of subtracting $n_o(\lambda, t)$ from $n_e(\lambda, t)$ and those resulting by maintaining the optical axis of the NLC at $\pi/4$ to the crossed polarizers emphasized a good agreement between these methods.

References

- [1] E. Dorn, Phys. Z. **11**, 777 (1910).
- [2] G. Pelzl, H. Sackmann, Symp. Faraday Soc. **5**, 68 (1971).
- [3] G. Pelzl, R. Rettig, D. Demus, Z. Phys. Chem. (Leipzig) **256**, 305 (1975).
- [4] O. Pellet, P. Chatelain, Bull. Soc. France Mineral. **73**, 154 (1950).
- [5] P. Chatelain, Bull. Soc. France Mineral. **78**, 262 (1955).
- [6] I. Haller, H. A. Huggins, M. J. Freiser, Mol. Cryst. Liq. Cryst. **16**, 53 (1972).
- [7] N. A. Vaz, G. W. Smith, G. P. Montgomery, W. D. Martin, Mol. Cryst. Liq. Cryst. **198**, 305 (1990).
- [8] H. Mada, S. Kobayashi, Mol. Cryst. Liq. Cryst. **33**, 47 (1976).
- [9] F. Kuschel, R. Rettig, G. Pelzl, D. Demus, Cryst. Res. Technol. **16**, 43 (1981).
- [10] M. Warengem, C. P. Grover, Rev. Phys. Appl. **23**, 1169 (1988).
- [11] M. Warengem, G. Joly, Mol. Cryst. Liq. Cryst. **207**, 205 (1991).
- [12] M. Socaciu, M. Ursache, Mol. Cryst. Liq. Cryst. **403**, 1 (2003).
- [13] M. F. Vuks, Opt. Spektrosk. **20**, 644 (1966).
- [14] S. T. Wu, Phys. Rev. A **33**, 1270 (1986).
- [15] S. T. Wu, J. Appl. Phys. **69**(4), 2080 (1991).
- [16] S. T. Wu, C. S. Wu, M. Warengem, M. Ismaili, Opt. Eng. (Bellingham) **32** (8), 1775 (1993).
- [17] J. Cognard, Alignment of Nematic Liquid Crystals and their Mixtures, Gordon & Breach Sci. Publ., New York (1982).
- [18] I. Palarie, Physics AUC **10**(1), 51 (2000).
- [19] L. D. Socaciu, C. Sarpe-Tudoran, S. Radu, M. Ursache, Annals of the University Bucharest **46**, 93 (1997).
- [20] M. Baniceru, S. Radu, C. Sarpe-Tudoran, Chromatographia **48**(5/6), 427 (1998).
- [21] J. D. Swalen, R. Santo, M. Tacke, J. Fischer, Polymers **21**(2), 168 (1977).